 CMES, vol.7, no.2, pp.207-222, 2005

Using radial basis functions in a "finite difference mode"

A.I.Tolstykh, D.A. Shirobokov [1]

Abstract: A way of using RBF as the basis for PDE's solvers is presented, its essence being constructing approximate formulas for derivatives discretizations based on RBF interpolants with local supports similar to stencils in finite difference methods. Numerical results for different types of elasticity equations showing reasonable accuracy and good h-convergence properties of the technique are presented. Applications of the technique to problems with non-self-adjoint operators (like those for the Navier-Stokes equations) are also considered.

keyword: radial basis functions, derivatives discretization, RBF schemes, solid mechanics equations, Navier-Stokes equations

1 Introduction

At present, high accuracy methods have a significant place in both theoretical investigations and applications due to their ability to serve, from one hand, as a high resolution numerical tools and, from another, as a fast solvers providing engineering accuracy. In the area of finite difference techniques, there exist families of high-order schemes which can be easily implemented into algorithms for solving various PDE. Unfortunately, their peak performance usually corresponds to the cases when high-quality smooth meshes can be constructed. Some times, it is not an easy task and considerable technical efforts are often required to do the job.

To circumvent the difficulties associating with meshing in the case of difference schemes, it was suggested [Tolstykh (2000)] to use them together with high-accuracy meshless approximations. In more detail, it was suggested to use the latter category in the framework of the domain decomposition strategy by partitioning a computational domain into "good" subdomains where smooth meshes can be easily generated and "bad" subdomains where scattered nodes can be used to discretize governing equations. Another possibility is using meshless approximations at junctions of smooth meshes generated for neighbour subdomains.

To match a meshless approximation with a finite difference one, it was proposed to use the former in a "finite difference mode" by introducing approximate formulas for derivatives using local interpolants. Radial basis functions were chosen for constructing the interpolants.

A hybrid scheme based on the 5th-order compact upwind differencing (CUD) approximations from [Tolstykh (1994)] and local MQ-RBF formulas was developed and successfully tested [Tolstykh (2000)].

Further investigations have shown that the proposed RBF technique can be quite accurate when used alone for solving certain classes of PDE's. The choice of RBF for meshless derivatives approximations was motivated by the existing results concerning the general properties of RBF interpolants and their applications to PDE's. In the context of the present approach, using RBF offers some nice possibilities

First, some RBF-based discretizations have potential for providing convergence rates dependent on exact solutions smoothness only rather than on degrees of underlying polynomial approximations in FD and FEM methods. In certain cases, they can be exponential. It fits neatly into the strategy of constructing arbitrary-order multioperators schemes [Tolstykh (2003)] exploiting exact solutions smoothness.

Second they can be easily implemented in PDE's solvers.

Third, good RBF performance in three-dimensional cases is theoretically expected.

At present, the most popular lines of attack when constructing RBF-PDE solvers seem to be collocation and boundary elements approaches [Fasshauer (1996)], [Franke and Schaback (1998)], [Kansa (1990)], [Zerroukat (1998)].

In [Wu and Shaback (1993)], [Wu (1998)] convergence proofs and error estimates of the collocation

[1] Computing Center of Russian Academy of Sciences, Moscow, Russia

procedure are presented. A profound impact on the RBF-collocation technique applications is due to papers [Kansa (1990)], [Kansa and Hon (2000)], [Sharan, Kansa and Gupta (1997)], [Wong, Hon, Li, Chung and Kansa (1999)]. In the works, much attention was given to Hardy's multiquadric [Hardy (1990)] with varying shape parameters. Dramatic increase of accuracy was found in the case of properly defined shape-parameter distributions.

The main difficulty when using RBF collocation approach is the necessity to invert ill-conditioned matrix arising due to a global RBF support. Several remedies to circumvent the problem were proposed. They are, in particular, domain decomposition approach [Wong, Hon, Li, Chung and Kansa (1999)], preconditioning and compactly supported RBF [Buhmann (1998)], [Wendland (1995)], [Wu (1995)]. Usinng local RBF supports in the framework of the differential quadratures approach was reported in [Shu et al. (2003)].

For completeness, an important class of mesh-free methods exploiting least-square type of approximation should be mentioned (the relevant references can be found, for example, in [Belytcko et al. (1996])]. Various forms of the meshless Petrov-Galerkin method can be found in [Atluri et al. (2004)], [Atluri and Shen (2002)], [Han and Atluri (2004)], [Atluri (2004)]. Another approach was to extend traditional concepts of finite difference methods to the case of irregularly spaced nodes thus preserving polynomial nature of the resulting approximations. Technically, the PDEs approximations can be constructed in several ways. To the best of our knowledge, the first attempt in this direction is dated back to [D'yachenko (1965)]. In the paper, irregularly spaced nodes were used to construct quadrature formulae defining solutions of the Lagrangian gas dynamics equations. Considerable development of the irregular spacing idea (with underlying polynomial basis) has been embodied in the Generalized Finite Difference Method (see [Lizka and Orkits (1978)] where approximations to derivatives were constructed using linear systems generated by Taylor expansion series, the main emphasize being placed on elliptical problems. The application of the similar idea to the Euler gas dynamics equations can be found in [Belotserkovskii and Kholodov (1999)].

The present paper concerns finite difference-type RBF schemes as a numerical tool for solving solid and fluid mechanics problems. Section 2 presents the description of RBF approximations to derivatives using compact supports (stencils) and the resulting schemes formed by algebraic equations resulting from approximations to governing equations at nodal points.

In section 3, the main concepts of finite difference schemes, that is, approximation, stability and convergence, are formulated for the present approach. As simplest examples showing the possibility of proving both approximation and stability and, hence, convergence, five-point stencils for the Poisson equation and three-point "upwind" and "downwind" stencils for advection equations are considered. A technique allowing to enlarge advection oriented stencils is outlined.

The rest of the paper presents numerical examples aimed mainly showing h-convergence of numerical solutions when using different types of stencils. The examples cover solid mechanics problems with known exact solution as well as solutions of model advection equations and the compressible Navier-Stokes equations.

2 RBF approximations to derivatives and RBF schemes

Suppose one has a set $X = \{\mathbf{x}_1, \mathbf{x}_2, \ldots, \mathbf{x}_M\} \subset \Omega$ of nodes in a computational domain Ω. Let $X_j = (\mathbf{x}_1^{(j)}, \mathbf{x}_2^{(j)}, \ldots, \mathbf{x}_{N_j}^{(j)}), X_j \subset X, \mathbf{x}_j \in X_j$ be a set of nodes surrounding each node $\mathbf{x}_j$. Following the finite difference terminology, the set will be referred to as a stencil corresponding to the node $\mathbf{x}_j$.

Suppose further that values $u_i = u(\mathbf{x}_i^{(j)})$ of a sufficiently smooth function $u(\mathbf{x}), \mathbf{x} \in \Omega$ are specified at some nodes $\mathbf{x}_k^{(j)}, k = 1, 2, \ldots, p$ of the jth stencil while functionals $Lu|_{\mathbf{x}=\mathbf{x}_k^{(j)}}$ generated by a linear operator L acting on $u(\mathbf{x})$ are given at $\overline{\mathbf{x}}_k^{(j)}, k = 1, 2, \ldots, q, \overline{\mathbf{x}}_k^{(j)} \in X_j$. It is assumed that $\mathbf{x}_i^{(j)}$ and $\overline{\mathbf{x}}_k^{(j)}$ are possibly coincident for certain i and k.

We construct the interpolant

$$s^{(j)}(\mathbf{x}) = \sum_{k=1}^{p} a_k \phi(||\mathbf{x} - \mathbf{x}_k^{(j)}||) + \sum_{k=1}^{q} b_k L\phi(||\mathbf{x} - \overline{\mathbf{x}}_k^{(j)}||) \quad (1)$$

$p,\ q \leq N_j$

Requiring that

$$s^{(j)}(\mathbf{x}_k^{(j)}) = u(\mathbf{x}_k^{(j)}), k = 1, 2, \ldots, p,$$

$$Ls^{(j)}|_{\mathbf{x}=\overline{\mathbf{x}}_k^{(j)}} = Lu|_{\mathbf{x}=\overline{\mathbf{x}}_k^{(j)}}, k = 1, 2, \ldots, q$$

one obtains a linear system for a_k, b_k. It reads

$$\begin{bmatrix} \phi_{11}...\phi_{1p} & L\phi_{11}...L\phi_{1q} \\ \vdots & \vdots \\ \phi_{p1}...\phi_{pp} & L\phi_{p1}...L\phi_{pq} \\ L\phi_{11}...L\phi_{1p} & L^2\phi_{11}...L^2\phi_{1q} \\ \vdots & \vdots \\ L\phi_{q1}...L\phi_{qp} & L^2\phi_{q1}...L^2\phi_{qq} \end{bmatrix} \begin{bmatrix} a_1 \\ \vdots \\ a_p \\ b_1 \\ \vdots \\ b_q \end{bmatrix} = \begin{bmatrix} u_1 \\ \vdots \\ u_p \\ Lu_1 \\ \vdots \\ Lu_q \end{bmatrix}$$

$\phi_{ik} = \phi(||\mathbf{x}_i^{(j)} - \mathbf{x}_k^{(j)}||)$, $L\phi_{ik} = L\phi(||\mathbf{x} - \mathbf{x}_k^{(j)}||)|_{\mathbf{x}=\mathbf{x}_i^{(j)}}$, $L^2\phi_{ik} = L^2\phi(||\mathbf{x} - \mathbf{x}_k^{(j)}||)|_{\mathbf{x}=\mathbf{x}_i^{(j)}}$, $u_i = u(\mathbf{x}_i^{(j)})$, $Lu_i = Lu|_{\mathbf{x}=\mathbf{x}_i^{(j)}}$.

The solvability of the above type of systems is widely discussed in the literature (see for example, survey [Kansa and Karlson (1995)]). It is proved [Madych and Nelson (1989)], [Micchelli (1986)] that the solvability holds for any distinct nodes distribution provided that $\phi(\mathbf{r})$ belongs to certain classes of functions. In particular, the systems are solvable in the case of multiquadrics RBF which is used in the present paper. Therein lies essential difference between Generalized Finite Difference Method (GFDM) and the present approach. Another difference can be seen from the following observation. In the GFDM case [Lizka and Orkits (1978)] the minimal number of equations needed to obtain "differencing" coefficients (and hence the minimal number of nodes in local supports) is uniquely defined by derivative orders and dimensions of spaces (2D or 3D). Adding more nodes leads to overdetermined sets of equations which require minimization of least squares functionals. In the present RBF case, the number of equations in the above system is defined by a chosen numbers p and q of the interpolation conditions in (1) so the minimal number of nodes is equal to $p+q$. Adding more nodes is also possible but in this case one has to solve overdetermined systems. Such possibility is discussed in Section 3.4.

Supposing now that D_α is the operator of the αth-order derivative in one direction or another at a node $\mathbf{x}_j$, and applying it to $s(\mathbf{x})$, one obtains the following "differencing" formulas for the $\mathbf{x}_j$ node

$$(D_\alpha u)_j \approx \sum_{k=1}^{p} C_k^{j,\alpha} u_k + \sum_{k=1}^{q} B_k^{j,\alpha} Lu_k,$$
$$u_k = u(\mathbf{x}_k^{(j)}), Lu_k = Lu|_{\mathbf{x}=\mathbf{x}_k^{(j)}} \quad (2)$$

where the coefficients $C_k^{j,\alpha}$ and $B_k^{j,\alpha}$ depend on the coordinates of the nodes forming the jth stencil.

Particular forms of Eq. (2) can be used for approximations to derivatives in governing equations. For example, a discrete forms of the first and second order x-derivatives of a function for j-th node reads

$$(u_x)_j \approx \sum_{k=1}^{p} C_k^{j,1} u_k, \quad (u_{xx})_j \approx \sum_{k=1}^{q} C_k^{j,2} u_k \quad (3)$$

where $C_k^{j,1}$ and $C_k^{j,2}$ are the RBf x-derivatives coefficients for the j-th stencil. Similar formulas can be constructed for higher derivatives. However, they can be also approximated by successive applications of RBF operators for lower order derivatives. One may also need derivatives discretizations near boundary nodes with the Neumann-type boundary conditions. A particular form of Eq. (2) can be written in this case as

$$(Du_\alpha)_j \approx \sum_{k=1}^{p} C_k^{j,\alpha} u_k + \sum_{k=1}^{q} B_k^{j,\alpha} (\partial u/\partial n)_k$$

where $(\partial u/\partial n)_k$ are boundary values of the normal to $\partial\Omega$ derivative. In the case of singular points, it is possible to modify the interpolant $s(x)$ in Eq. (1) for stencils near singularities. It can be accomplished by considering u as a product of singular and non-singular functions and interpolating the latter.

Discretization at each node of a given PDE can be proceeded in a standard finite difference manner by changing derivatives by their approximations. Assembling then the resulting algebraic equations and using boundary conditions (which, if needed, can be discretized as well provided that they contain derivatives), one obtains a global system for unknown nodal variables. In the linear case, its matrix is a sparse one, the condition numbers for "global" systems being found to be quite acceptable. It facilitates convergence of standard iterative methods of their solutions. However, in the numerical experiments described below, mainly the direct nested dissection method [George and Liu (1981)] was used.

It should be noted that though the present technique suggests $N_j << M$, ill-conditioning of systems for determining the coefficients in Eq. (2) can not be ruled out if N_j is too large or distances between nodes are too small. In the calculations, the situation has been encountered only in the h-convergence studies when very small values of h, the characteristic distances between nodes, were used. In those cases, quadro precision arithmetic was exploited.

Summing up, to solve a PDE using the present RBF approach, one should:
(i) Specify a nodal distribution in the considered computational domain;
(ii) For each node $\mathbf{x}_j$ considered as a center, specify stencils with N_j nodes surrounding $\mathbf{x}_j$;
(iii) For each stencil, obtain "differencing" coefficients (for example $C_k^{j,\alpha}$ and $B_k^{j,\alpha}$ in (2)) by solving linear systems;
(iv) Substitute the approximations to derivatives at each node in the PDE, taking into account the relevant boundary conditions, and form the resulting "global" system by assembling together the nodal approximations;
(v) Solve the global system.

It should be noted that steps (i)-(iii) can be viewed as a preprocessing procedure once nodal distributions and stencils are not supposed to be changed during calculations. In nonlinear cases, only steps (iv) and (v) have to be included in iterations.

The approach seems to possess the following merits.
(i) The problem of ill conditioned systems is greatly relaxed due to a limited number of nodes in stencils.
(ii) The technique has the potential for being quite accurate.
(iii) Once RBF coefficients of the derivatives approximation are calculated, the technique can be implemented in a simple manner typical for finite difference schemes.
(iv) The approach offers considerable flexibility by constructing various stencil configurations for different center nodes where derivatives are considered (for example, special configurations near boundaries and singularities).
(v) The resulting RBF schemes can be readily combined with finite differencing schemes in the framework of the domain decomposition strategy.

3 Approximation, stability and convergence

Main definitions and theorems of the finite difference schemes theory can be readily applied to the present RBF approach. We present them in spirit of [Godunov and Ryaben'kii (1977)].

Consider a target problem written in the abstract form

$$Lu = f, \;\; u \in U, \;\; f \in F \tag{4}$$

where U and F are spaces to which belong the solution u and RHS f.

Suppose we have a RBF discretization of Eq. (4) written in the form

$$L_{RBF} u_h = f_h, \;\; u_h \in U_h, \;\; f_h \in F_h \tag{5}$$

where the index h denotes nodal functions and spaces of nodal functions. We also denote by h some character distance between nodes, for example,

$$h = \max_j \max_i ||\mathbf{x}_i^{(j)} - \mathbf{x}_j||$$

where $\mathbf{x}_j$ is a center of the j-th stencil where derivatives are approximated. We supposed that both U_h and F_h spaces are supplied by norms $||\cdot||_{U_h}$ and $||\cdot||_{F_h}$. Following notations from [Godunov and Ryaben'kii (1977)], we introduce a projection operator $[\cdot]_h : \; U \to U_h$ which can be viewed as a table of values of $u \in U$ at nodal points $\mathbf{x}_j \in X (j = 1, ..., M)$.

Definition 1
RBF scheme (5) approximates target problem (4) with an order k if

$$||L_{RBF}[u]_h - f_h||_{F_h} < \varepsilon(h), \quad \varepsilon(h) = O(h^k) \tag{6}$$

According to the above definition, the approximation property of Eq. (5) can be established by considering the action of L_{RBF} on solution of Eq. (4) at the nodal points and then checking if the difference between the result and f_h tends to zero as h^k when h tends to zero. In practice, there is no need in knowing the exact solution $u(x)$. It is sufficient to use its smoothness properties and possibly the equality $Lu - f = 0$. Technically, one should construct the Taylor expansion series for $L_{RBF}[u]_h$ at the nodes and see if the zero order terms form the exact operator plus $O(h^k)$ remainder. Of course, one should check also if f_h approximates f with the $O(h^k)$ order but usually it is natural to set $f_h = [f]_h$.

Unfortunately, the procedure is more complicated than that in the finite difference case since analytical expressions for the RBF coefficients $C_k^{j,\alpha} j$ and $B_k^{j,\alpha} j$ in Eq. (2) are needed.

Definition 2
The RBF scheme Eq.(5) is said to be stable if:
(i) Eq. (5) is solvable for u_h, f_h being an arbitrary nodal function,
(ii) the following inequality holds

$$||u_h - v_h||_{U_h} < C_1 ||\delta_h||_{F_h}$$

where v_h and δ_h are the solution and the perturbation respectively of the perturbed equation

$$L_{RBF} v_h = f_h + \delta_h$$

while constant C_1 is independent of h.

The above definition is formulated for general case of a non-linear problems (4). In the case of a linear L_{RBF} it is equivalent to

$$||L_{RBF}^{-1}|| < C_2 \text{ or } ||u_h|| < C||f_h|| \tag{7}$$

where C_2 and C are independent of h. To prove the equivalence of (ii) and (7), it is sufficient to use the definition of norms of any operator $A: U_h \to F_h$ which looks as

$$||A|| = \sup_{v \neq 0} \frac{||Av||_{F_h}}{||v||_{U_h}}$$

and the equality $u_h - v_h = L_{RBF}^{-1}\delta_h$.

Theorem 1

Suppose RBF scheme (5) approximates problem (4) with an order and is stable. Than its solution tends to the exact solution at nodes as $O(h^k)$ when $h \to 0$ and the following estimate holds

$$||[u]_h - u_h|| < C_1 \varepsilon(h),\ \varepsilon(h) = O(h^k) \tag{8}$$

where C_1 is independent of h.

Proof

Consider the following pair of equation

$$L_{RBF} u_h = f_h$$

$$L_{RBF}[u]_h = f_h + \delta_h$$

One has due to the stability of the scheme

$$||[u]_h - u_h|| < C_1||\delta_h||.$$

But $||\delta_h|| < \varepsilon(h)$ due to the approximation property Eq. (6). Therefore the convergence inequality holds with $\varepsilon(h) = O(h^k)$.

In general, the most difficult part of theoretical investigation of the present type of RBF schemes seems to be stability proofs. The situation is quite similar to that in the area of difference schemes. It is quite understandable since they may be viewed as the important step towards proving exact solutions existence. However in some simple linear cases of uniformly distributed nodes and small number of nodes in stencils, it is possible to prove both approximation and stability statements and hence to prove convergence to exact solution with increasing density of nodes. As particular cases, we present below simple examples.

In the following, the Hardy multiquadrics (MQ) radial basis functions will be considered only, the constant C in their definition being set to unity. Of course, judging from the investigations [Kansa (1990)], [Kansa and Hon (2000)], the present solutions accuracy is expected to be poorer than that for a more successful choice of C.

3.1 Five point stencils for the Laplace operator

Consider the standard stencil used in the second order finite difference schemes for the Poisson equation. In the case of an uniform mesh with the mesh step h, it contains four nodes near each center x_{ij}, that is nodes $x_{i\pm1,j\pm1}$. For such stencils, it is possible to obtain the analytical solution for the coefficients $C_k^{j,2}$ in (3) and then to expand them in terms of the mesh size. Omitting upper indices, the result for the second x-derivatives and the numbering shown in Fig. 1a looks as

$$c_1 = -\frac{2}{h^2} + \frac{5}{3} + O(h^2),\ c_2 = c_4 = -\frac{1}{h^2} - \frac{7}{6} + O(h^2),$$

$$c_3 = c_5 = \frac{1}{3} + O(h^2)$$

As seen, the difference in the RBF and 5-point FD approximations to the second derivatives is of $O(h^2)$ order. Using two lower indices notations, the RBF approximation to the Laplace operator can be cast in the form

$$\Delta_{RBF} u_{ij} = (1 - \frac{5}{6}h^2)\Delta_{FD} u_{ij} + c_{ij}h^2 + O(h^4) \tag{9}$$

where

$$c_{ij} = -\frac{7}{6}u_{ij} + \frac{1}{12}\left(\frac{\partial^4 u}{\partial x^4} + \frac{\partial^4 u}{\partial y^4}\right)_{ij}$$

and $\Delta_{FD} u_{ij}$ is the second-order accurate five-point finite difference operator.

Consider now the Dirichlet problem

$$\Delta u = f(x,y),\ x,y \in \Omega \setminus \partial\Omega \tag{10}$$

$$u|_{\partial\Omega} = \phi(x,y)|_{x,y\in\partial\Omega} = \phi_\Gamma \tag{11}$$

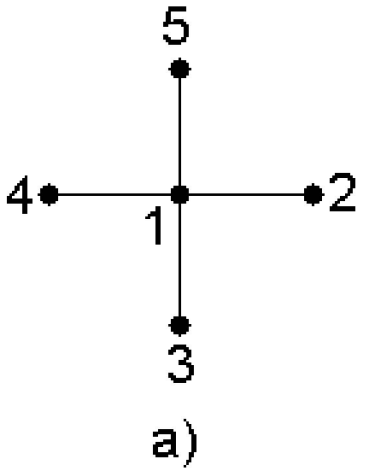

Figure 1 : Examples of stencils for low-order approximations.

Introducing the uniform mesh $\omega_h = (x_i = ih,\ y_j = jh)$ the five point discretization of (10), (11) can be written as

$$\Delta_{RBF} u_{ij} = f_{ij},\ (x_i, y_j) \in \omega_h = \Omega_h \backslash \Gamma_h \tag{12}$$

$$u_{ij}|_{\Gamma_h} = \phi_{\Gamma_h},\ \ (x_i, y_j) \in \Gamma_h \tag{13}$$

In Eq. (12) and (13), Ω_h is the set of nodes $x_i, y_j \in \Omega$ and Γ_h is a set of boundary and possibly near boundary nodes were $u_{ij}|_{\Gamma_h}$ are supposed to be defined by (13) in one way or another.

Theorem 2

RBF scheme (12) and (13) is stable for sufficiently small h.

Proof

The proof is similar to that in the case of finite difference operator Δ_{FD} (for example, [Godunov and Ryaben'kii (1977)]), only slight modification being needed. It is based on the following observations

(I)

$$\Delta_{RBF}(x^2+y^2)_{ij} = 4\left(1 - \frac{5}{6}h^2\right) + O(h^2) \tag{14}$$

(II) Supposing that $f(x,y) > 0$, the nodal function u_h satisfying (12) can not have its maximum value when $(x_i, y_j) \in \omega_h$ at least for sufficiently small h.

Statement (I) follows from (9) while (II) can be proved in the following way. Consider Eq. (9). Using the standard FD notation, Eq. (12) can be rewritten as

$$(u_{i+1,j} + u_{i-1,j} + u_{i,j+1} + u_{i,j-1} - 4u_{ij}) = \frac{c_{ij}h^4}{1 - \frac{5}{6}h^2} + \frac{h^2 f_{ij}}{1 - \frac{5}{6}h^2} + O(h^6) \tag{15}$$

Now suppose that there exists a node $x_{\tilde{i}}, y_{\tilde{j}}$, $(\tilde{i}, \tilde{j}) \in I(\omega_h)$ satisfying $\max_{i,j \in I(\Omega_h)} u_{ij} = u_{\tilde{i}\tilde{j}}$ where $I(\omega_h)$, $I(\Omega_h)$ are the index sets corresponding to ω_h, Ω_h respectively.

Considering Eq.(15)) for $i = \tilde{i},\ j = \tilde{j}$, one can see that it can not be satisfied for sufficiently small h since the LHS of (15) is negative due to our assumption while its RHS is positive due to $f_{\tilde{i}\tilde{j}} > 0$. Hence, our assumption is erroneous.

Returning now to Eq.(12) , we construct the nodal function

$$v_{ij} = u_{ij} + \frac{d}{2}(x^2+y^2)_{ij} \max_{i,j \in I(\omega_h)} |f_{ij}|$$

where constant $d > 1$ is chosen to satisfy $d > x^2 + y^2$, $x^2 + y^2 \in \Omega$. One has the following equation

$$\Delta_{RBF} v_{ij} = \Delta_{RBF} u_{ij} + 2d\left(1 - \frac{5}{6}h^2\right) \max_{i,j \in I(\omega_h)} |f_{ij}| + O(h^2) \tag{16}$$

Since the first term in the RHS of (16) is f_{ij}, one can see that the RHS is positive for sufficiently small h. So one has due to (II) $v_{ij} < v|_{\Gamma_h}$. Using then the expressions for $v|_{\Gamma_h}$, one obtains

$$u_{ij} < \frac{d}{2}(x^2+y^2)|_{\Gamma_h} \max_{i,j \in I(\omega_h)} |f_{ij}| + \max_{\Gamma_h} |\phi_\Gamma| <$$

$$\frac{d^2}{2} \max_{i,j \in I(\omega_h)} |f_{ij}| + \max_{\Gamma_h} |\phi_\Gamma|$$

for sufficiently small h. Multiplying Eqs. (12), (13) by (-1) and repeating the above reasoning, one arrives at the last inequality written for $-u_{ij}$. Hence, it is true for $|u_{ij}|$. We define now the following norms

$$||u_h||_{U_h} = \max_{i,j \in I(\omega_h)} |u_{ij}|,$$

$$||f_h||_{F_h} = \max_{i,j \in I(\omega_h)} |f_{ij}| + \max_{\Gamma_h} |\phi_\Gamma|$$

and obtain $\max_{ij \in \omega_h} |u_{ij}| = ||u_h||_{U_h} \le C||f_h||_{F_h}$ where $C = max\left(1, d^2/2\right)$. It means that scheme (12), (13) is stable in maximum norm.

3.2 Three-point stencil for the advection equation

Consider first the RBF approximation to $\partial u/\partial x$ using three point "upwind" and "downwind" stencils shown in Fig. 1b, 1c, the nodes numbering and geometrical parameters being presented herein.

In the case of upwind stencil Fig. 1b, the analytical expressions for the RBF coefficients $C_1,\ C_2,\ C_3$ in the approximate formula

$$D^+u_1 = \sum_{i=1}^{3} C_i u_i \approx \left(\frac{\partial u}{\partial x}\right)\Big|_{x=x_1,y=y_1}$$

lead to the following estimates

$$\begin{aligned} C_1 &= \frac{ksin\beta + sin\gamma}{sin(\beta+\gamma)kh} + O(h), \\ C_2 &= -\frac{sin\beta}{sin(\beta+\gamma)h} + O(h) \\ C_3 &= -\frac{sin\gamma}{2sin(\beta+\gamma)kh} + O(h), \\ C_1 + C_2 + C_3 &= h\frac{sin\beta + ksin\gamma}{2sin(\beta+\gamma)} \end{aligned} \tag{17}$$

It follows from (17) that

$$C_1 > 0,\ C_2 < 0,\ C_3 < 0,\ C_1 = |C_2| + |C_3| + \delta,\ \delta > 0 \tag{18}$$

for sufficiently small h. Moreover, the Taylor expansion series give

$$D^+u_1 = \left(\frac{\partial u}{\partial x}\right)_{x=x_1,y=y_1} - h\left(Au + B\frac{\partial^2 u}{\partial x^2} + C\frac{\partial^2 u}{\partial y^2} + D\frac{\partial^2 u}{\partial x \partial y}\right)_{x=x_1,y=y_1} + O(h^2) \tag{19}$$

where $A,\ B,\ C,\ D$ are functions of $\alpha,\ \beta,\ k$ satisfying $A < 0,\ B > 0,\ C > 0$. It is possible to show also that $4BC - D^2 = sin^2(\beta+\gamma) > 0$ which means that the strong ellipticity condition $B\xi^2 + C\eta^2 > 2D\xi\eta$ is satisfied. It means that (19) is the first-order dissipative approximations to $\partial u/\partial x$ like that in the case of the two-point backward finite difference approximation to the derivative.

In the case of the downwind stencil Fig. 1c, the estimates similar to (17) can be obtained by the substitutions $\beta \to \alpha + \pi,\ \gamma \to \gamma + \pi$. Eq.(19) then should be changed by changing D^+ by D^-in the LHS and changing minus by plus in the RHS without changing expressions for $A,\ B,\ C,\ D$.

An important property of D^+ (D^-) operators is the positivity (negativity) of their components in the case of the nodal distribution generated by the uniform skewed mesh.

Consider the mesh shown in Fig. 1d with the cells formed by the upwind stencil, Fig. 1b, in a skewed coordinate system (ξ, η). We introduce now two-indices notations for a nodal functions, that is $u_{ij} = u(x_{ij}, y_{ij})$ where x_{ij}, y_{ij} are the Cartesian coordinates of nodes $\xi_i = hi$, $\eta_j = khj$, $i, j = 0, \pm1, \pm2, ...$ We introduce also the Hilbert space of nodal functions defining the inner product

$$(u_h, v_h) = h^2 \sum_{i,j=-\infty}^{\infty} u_{ij} v_{ij}$$

Theorem 3
The D^+ operator satisfies $(D^+u_h, u_h) > 0$.

Proof
Let us define the following operators

$$\begin{aligned} &\Delta^{(k)} = I - T_{-1}^{(k)},\ \Delta_0^{(k)} = T_1^{(k)} - T_{-1}^{(k)}, \\ &\Delta_2^{(k)} = T_1^{(k)} - 2I + T_{-1}^{(k)},\ k = 1,2 \end{aligned} \tag{20}$$

where $T_l^{(1)}$ and $T_l^{(2)}$ are the shift operators corresponding to the ξ and η coordinates respectively, that is, $T_l^{(1)} u_{ij} = u_{i+l,j}$, $T_l^{(2)} u_{ij} = u_{i,j+l}$. Now it is easy to see that $\Delta^{(k)} = \frac{1}{2}(\Delta_0^{(k)} - \Delta_2^{(k)})$. One can also verify by shifting the summation indices that $\Delta_0^{(k)}$ and $\Delta_2^{(k)}$ satisfy

$$(\Delta_0^{(k)} u_h, u_h) = 0,\ (\Delta_2^{(k)} u_h, u_h) = -h^2 \sum_{i,j=-\infty}^{\infty} (\Delta^{(k)} u_{ij})^2,$$

$k = 1,2$

which means that they are the skew-symmetric and the self-adjoint negative components of $\Delta_0^{(k)}$ respectively.

Using the two-indices notations for the action of D^+, one has $D^+u_{ij} = C_1 u_{ij} - |C_2| u_{i-1,j} - |C_3| u_{i,j-1}$ or $D^+u_{ij} = |C_2|\Delta^{(1)}u_{ij} - |C_3|\Delta^{(2)}u_{ij} + \delta u_{i,j}$. The calculations of the inner product give

$$h^{-2}(D^+u_h, u_h) = |C_2| \sum_{i,j=-\infty}^{\infty} (\Delta^{(1)} u_{ij})^2 +$$

$$|C_3| \sum_{i,j=-\infty}^{\infty} (\Delta^{(2)} u_{ij})^2 + \delta \sum_{i,j=-\infty}^{\infty} u_{ij}^2 > 0$$

for sufficiently small h.

In the same way, it can be proved that $(D^{-}u_h, u_h) < 0$.

Consider now the 2D advection equation

$$\frac{\partial u}{\partial t} + a\frac{\partial u}{\partial x} + b\frac{\partial u}{\partial y} = 0,\ a,b = const. \tag{21}$$

There are two ways of using the RBF derivatives approximations formed by 3-point stencils.

First, one can use x- and y- upwind or downwind derivatives stencils separately according to the a and b signs (that is, upwind or downwind for the positive or negative coefficients respectively). Second, one can cast Eq. (21) in the "unidirectional" form by writing

$$\frac{\partial u}{\partial t} + c\frac{\partial u}{\partial \xi} = 0$$

where ξ is the coordinate along the advection direction which makes the angle ϕ with the x-axes defined by $\phi = arctg\ b/a$. Then the operators $D^{\pm}$ may be viewed as a 3-point approximation to the ξ-derivative when substituting $\beta \to \beta + \phi$, $\gamma \to \gamma - \phi$ in Eqs.(17). Of course, nodes 2 and 3 in Fig. 1b, 1c should be chosen to meet the conditions $\beta < \pi/2$, $\gamma < \pi/2$. In both cases, the spatial RBF discretizations lead to positive operators and, as can be easily shown, result in conditionally or unconditionally stable schemes (depending on chosen time stepping procedures).

Of course, using the above stencils in the case of arbitrary spaced nodes and $a = a(x,y,u)$, $b = b(x,y,u)$ may be viewed as a good heuristic choice based on the "frozen coefficients" and "frozen nodal distribution" principles.

Unfortunately, analytic investigations into RBF schemes in the case of arbitrary spaced nodes are quite complicated if the number of nodes in stencils is large. It is the case if one wants to construct high accuracy discretization. So numerical experiments play an important role when estimating the efficiency of the present technique.

3.3 Comments in using irregularly spaced nodes.

Though the present technique (as other meshless methods) can enjoy operating with arbitrary node distributions, nodes spacings may influence significantly accuracy of numerical solutions. For example, concentration of nodes is needed in regions where exact solutions gradients are large. In this way, approximation errors $\varepsilon(h)$ in Eq. (6) can be decreased. From the practical viewpoint, it is advantageous in many cases to borrow nodal distributions from either FEM or FD meshes and modify them (if needed) in a desired manner (for example. by adding more nodes, rearranging nodes and/or allowing them to move during calculations).

Supposing that a proper nodal distribution is specified, one encounters the necessity of defining stencils. As in the case of finite difference methods, the resulting RBF schemes should meet the stability requirements. Otherwise two calculation scenarios are possible. The first one is a breakdown of time stepping or iterative procedures. The second (and perhaps more dangerous) possibility is obtaining a solution for a fixed nodes distribution which bears no relation to the corresponding exact one.

It means that in the cases for which stability proofs are lacking, calculations with increasing densities of nodes are needed to demonstrate convergence to exact solutions. The results of calculations of this sort for PDEs relevant to elasticity problems have shown that various geometrical forms of supports are possible.

It is not the case if one deals with non-selfadjoint operators in convection, convection-diffusion or fluid dynamics types of equations. As for finite difference methods, a choice of supports is of prime importance when constructing stable RBF schemes. In this context, the properties of the above described three-point stencils may serve as guidelines. An example is presented below.

3.4 Heuristic upwind-type stencils

The three-point stencils described in the previous subsection provide low-order approximations. A way of constructing more accurate RBF formulas for advection terms is as follows. Suppose that one has a stencil with p nodes but only $l < p$ equations are used to obtain the RBF operator. Assuming that the differencing formula

$$\left.\frac{\partial u}{\partial x}\right|_{\mathbf{x}=\mathbf{x}_j} \approx D^{h+}u_j = \sum_{i=1}^{p} c_i^{+} u_i \tag{22}$$

is identically accurate for l RBF $\phi(||\mathbf{x} - \mathbf{x}_k^{(j)}||)$, $k = 1,...,l$, one arives at the system

$$\left.\frac{\partial \phi(||\mathbf{x} - \mathbf{x}_k^{(j)}||)}{\partial x}\right|_{\mathbf{x}=\mathbf{x}_j} = \sum_{i=1}^{p} c_i^{+} \phi(||\mathbf{x}_i^{(j)} - \mathbf{x}_k^{(j)}||) \tag{23}$$

$k = 1,...,l$

If $l = p$ then the coefficients c_i^{+} are those obtained using the interpolation conditions at $\mathbf{x} = \mathbf{x}_j$, $j = 1,...,l$. In our

case $l < p$ and system(22) has an infinite set of solutions. They can be written as

$$c_i^+ = a_i + \sum_{q=1}^{p-l} b_{iq} t_q,\ i = 1, ..., p \tag{24}$$

where $t_q,\ q = 1, .., p-l$ are free parameters while a_i, b_{iq} are uniquely defined.

Suppose now that a three-point upwind stencil with the center $\mathbf{x}_j$ is specified which gives C_1, C_2 and C_3 coefficients. Then we define the p-component vector $(\tilde{c}_1, \tilde{c}_2, ..., \tilde{c}_p) = (C_1, C_2, C_3, 0, ..., 0)$ corresponding to the nodes $\mathbf{x}_1^{(j)}, \mathbf{x}_2^{(j)}, ..., \mathbf{x}_p^{(j)}$ and require that

$$\sum_{i=1}^{p} (c_i^+ - \tilde{c}_i)^2 = min \tag{25}$$

In other words, we require that c_i^+ coefficients are close to $\tilde{c}_i$ in the least square sense. Substituting Eq.(24) into Eq.(25) and differentiating the result in respect to $t_q,\ q = 1, .., p-l$, we arrive at a linear system defining c_i^+. Euristically, we expect that "upwinding property" of c_i are close to that of C_1, C_2, C_3.

4 Numerical examples

4.1 Derivatives approximation accuracy

A natural but not general way to estimate the approximation errors of "differencing" formulas (2) is direct calculations for certain classes of functions. Of coarse, it gives only some impression concerning the RBF performance in a finite difference mode. The results of the calculations for MQ interpolants with appended constant are presented in [Tolstykh (2000)]. Fig. 2 shows the absolute values of errors in the case of first and second derivatives of $f(x) = \exp(2(x+y))$ for $x = 0$, $y = 0$ when using the stencils indicated herein.

It can be seen from Fig. 2 that the errors can be well presented by the power laws h^p where h is the distance between nodes while $p = 2,\ 4,\ 6$ for stencils $1, 2, 3$. For a fixed $h = h_*$, enlarging stencils increases the accuracy of the derivatives discretization. However, one should not expect that this will continue when the number of nodes $N_j = K$ in the stencils increases without bound. When $K \to \infty$, the accuracy of the interpolation which provides differencing formulas is expected to tend to that of the cardinal interpolation [Buhmann (1990)] for $h = h_*$.

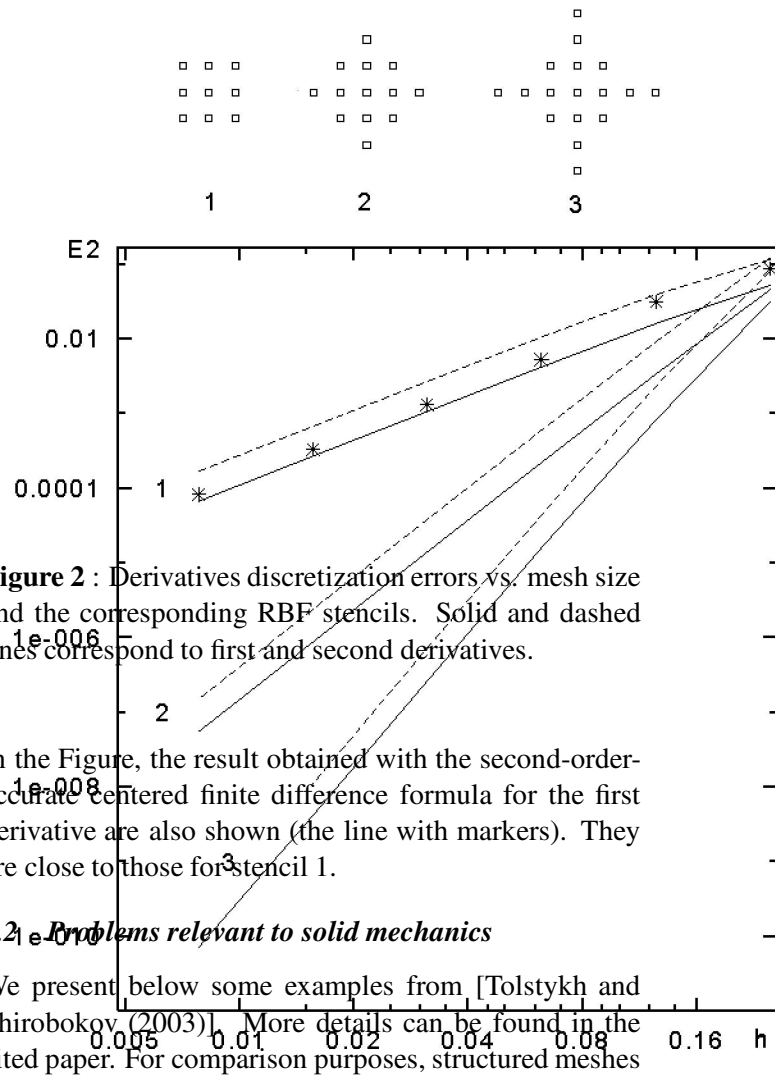

Figure 2 : Derivatives discretization errors vs. mesh size and the corresponding RBF stencils. Solid and dashed lines correspond to first and second derivatives.

In the Figure, the result obtained with the second-order-accurate centered finite difference formula for the first derivative are also shown (the line with markers). They are close to those for stencil 1.

4.2 Problems relevant to solid mechanics

We present below some examples from [Tolstykh and Shirobokov (2003)]. More details can be found in the cited paper. For comparison purposes, structured meshes served in many cases as generators of nodal distributions.

Poisson equation. We consider first the Dirichlet's problem for the Poisson equation appearing for example when considering bars torsion. The problem is

$$\triangle u = f(x,y) = -2\pi^2 \sin\pi x\ \sin\pi y,$$

$$\Omega = \{0 < x < 1,\ 0 < y < 1\},\ u|_{\partial\Omega} = 0$$

The exact solution is $u = \sin\pi x\ \sin\pi y$. As RBF nodes, those of meshes usually adopted for FD and FEM calculations were used thus facilitating comparisons of the solutions on equal terms. As a particular examples of constructing stencils, two types of supports for each center nodes with 7 and 19 neighbour points supplied by triangulated meshes were considered. They will be referred to as "simple" and "enlarged" ones

Fig. 3 presents the discrete L_2 norms of the solutions errors for the "simple"(RBF-1) and "enlarged"(RBF-2)

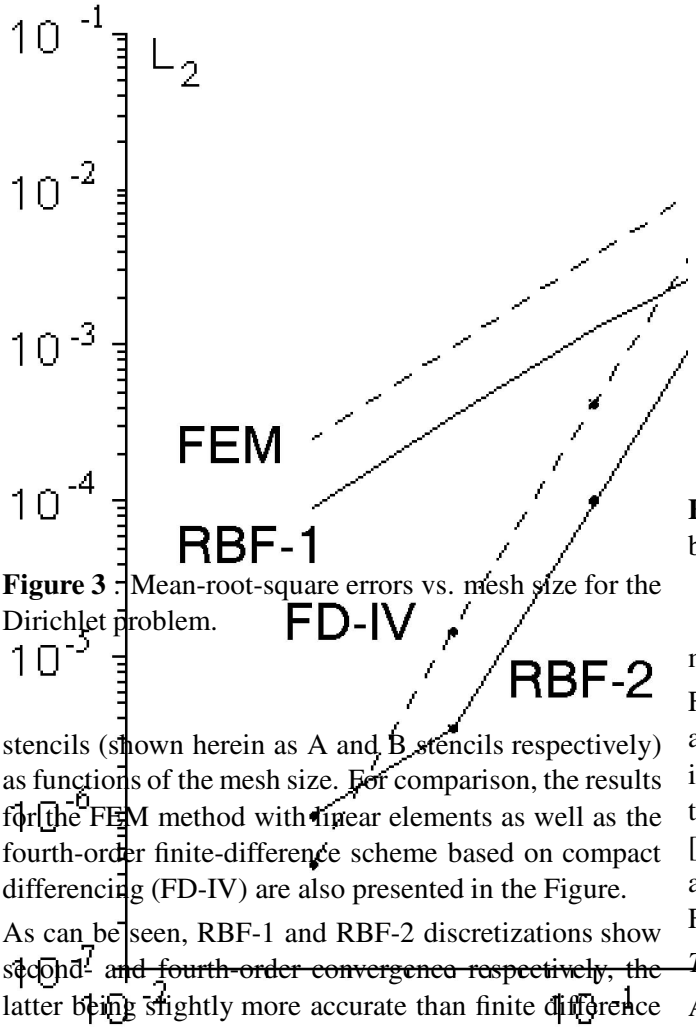

Figure 3 : Mean-root-square errors vs. mesh size for the Dirichlet problem.

stencils (shown herein as A and B stencils respectively) as functions of the mesh size. For comparison, the results for the FEM method with linear elements as well as the fourth-order finite-difference scheme based on compact differencing (FD-IV) are also presented in the Figure.

As can be seen, RBF-1 and RBF-2 discretizations show second- and fourth-order convergence respectively, the latter being slightly more accurate than finite difference one. Some decrease of accuracy of the RBF-2 solution seen in the finest mesh region is perhaps due to the deterioration of the condition number of the linear systems defining the RBF operator.

Biharmonic equation: bending of simply supported rhombic plate under an uniform load. In this case, there is a singularity of the exact solution which has an adverse effect on accuracy of a numerical method due to decreasing its smoothness with decreasing the angle α, $\alpha < \pi/2$, of the rhomb. More presicely, the asymptotic behaviour of the exact solution near corner points looks like $O(r^{\nu})$, $\nu = \pi/(\pi - \alpha)$, where r is the distance from the corner point.

The problem is investigated in [Babuska and Scapolla (1989)] in the context of several finite element methods performance using the variational approach rather than the biharmonic equation.

In the present calculations, nodal distributions from uniform triangulations were used, no special RBF approximations near corners being introduced.

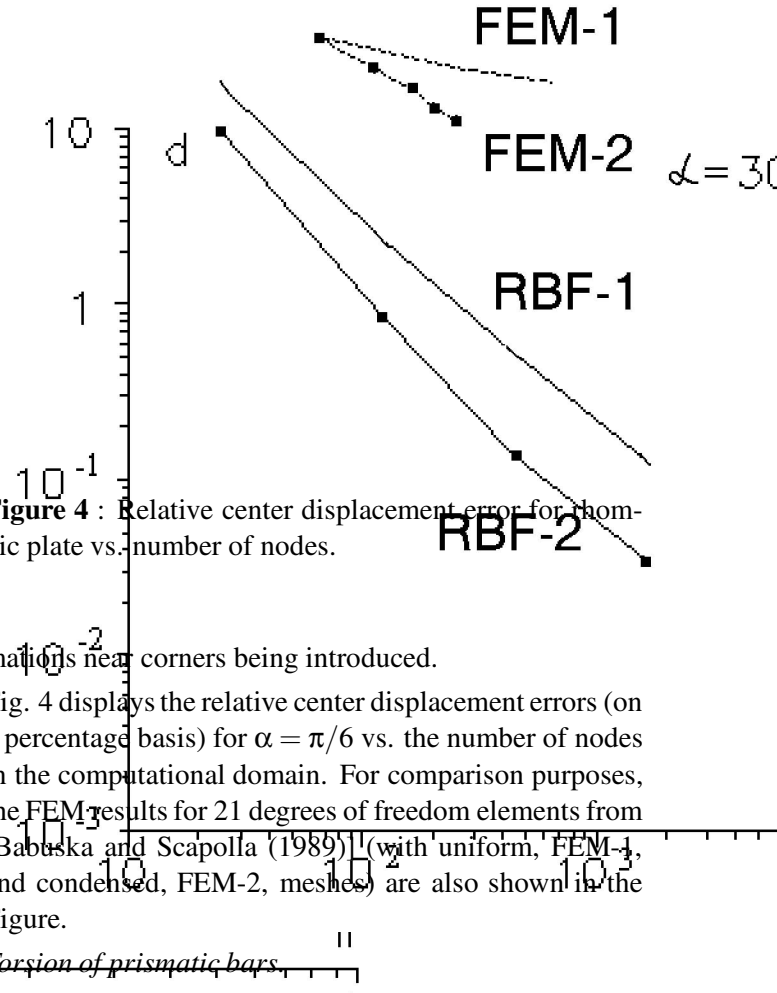

Figure 4 : Relative center displacement error for rhombic plate vs. number of nodes.

Fig. 4 displays the relative center displacement errors (on a percentage basis) for $\alpha = \pi/6$ vs. the number of nodes in the computational domain. For comparison purposes, the FEM results for 21 degrees of freedom elements from [Babuska and Scapolla (1989)] (with uniform, FEM-1, and condensed, FEM-2, meshes) are also shown in the Figure.

Torsion of prismatic bars.

According to the elasticity theory, solutions of the bar torsion problem can be obtained by solving the Dirichlet problem for the Poisson equation

$$\triangle\phi = -2,\ \mathbf{x} \in \Omega,\ \phi|_{\partial\Omega} = 0$$

where Ω is a bar cross-section domain. The corresponding stress components can then be expressed in terms of x- and y-derivatives of ϕ. In the case of cross-sections which boundaries contain "incoming" angles with rounded vertices, it is of interest to predict accurately stress concentrations near rounded corners where high gradients are possible (it has been known that stresses become singular when the corresponding curvature radii tend to zero).

We consider the geometry of a bar cross-section shown in Fig. 5 which was investigated in [Vlasov and Volkov (1995)] using very accurate semi-analytic method. The cross section is characterized by the radius r of the rounded corner and the "shelf" length A, the shelf thickness being assumed to be unity. To describe properly

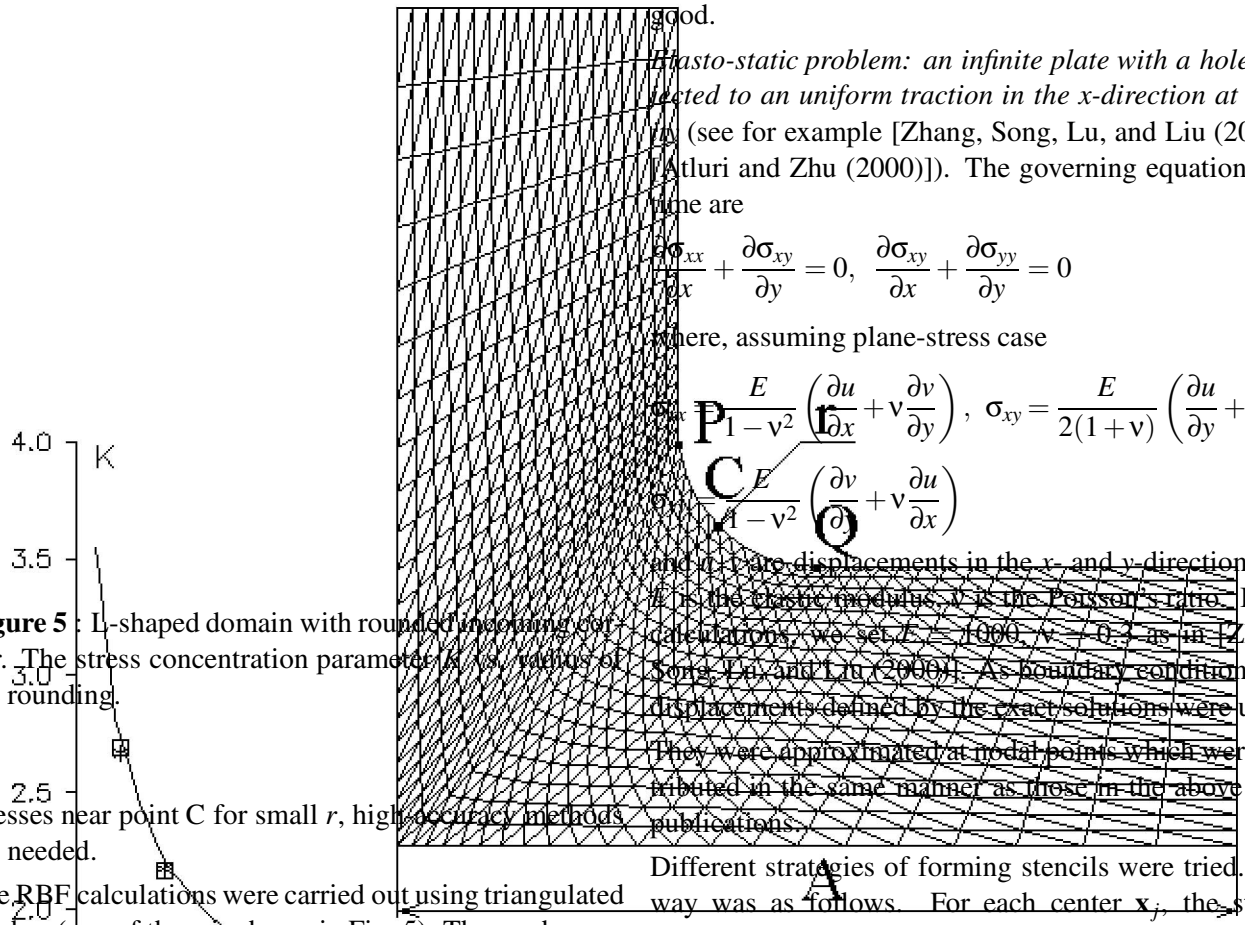

Figure 5 : L-shaped domain with rounded incoming corner. The stress concentration parameter K vs. radius of the rounding.

stresses near point C for small r, high-accuracy methods are needed.

The RBF calculations were carried out using triangulated meshes (one of them is shown in Fig. 5). The meshes are defined by numbers M and N of nodes uniformly distributed along the boundary PQ and the boundary RS respectively. Thus the condensing of nodes near C can be achieved by increasing M. The mesh shown in Fig. 5 is defined by $M = 11, N = 20$.

To compare the solution $K = grad\ \phi$ gradient in C with the results of [Vlasov and Volkov (1995)], the ϕ derivatives were approximated using the third-order four-points formula. The calculations carried out for three meshes $M \times N = 11 \times 20,\ 21 \times 40,\ 41 \times 80$ showed that the difference between the results corresponding to the second and the third meshes can be estimated as 0.2%.

Fig. 5 displays the K values obtained for $A = 3$ and $r = 0.5,\ 0.3,\ 0.1,\ 0.05$ using the "simple" stencil defined on the coarsest mesh (markers as squares) and finest mesh (markers as stars), the difference between the values being about 1.2%. (an exception is the case $r = 0.05$).

The curve depicted in Fig. 5 corresponds to the "almost exact" solution for $A = \infty$. Since the influence of A is quite insignificant in the domain $A > 3$ (the results for $A = 3$ and $A = 4$ differs by 0.2%), the agreement is rather good.

Elasto-static problem: an infinite plate with a hole subjected to an uniform traction in the x-direction at infinity (see for example [Zhang, Song, Lu, and Liu (2000)], [Atluri and Zhu (2000)]). The governing equations this time are

$$\frac{\partial \sigma_{xx}}{\partial x} + \frac{\partial \sigma_{xy}}{\partial y} = 0, \quad \frac{\partial \sigma_{xy}}{\partial x} + \frac{\partial \sigma_{yy}}{\partial y} = 0$$

where, assuming plane-stress case

$$\sigma_{xx} = \frac{E}{1-\nu^2}\left(\frac{\partial u}{\partial x} + \nu \frac{\partial v}{\partial y}\right), \quad \sigma_{xy} = \frac{E}{2(1+\nu)}\left(\frac{\partial u}{\partial y} + \frac{\partial v}{\partial x}\right),$$

$$\sigma_{yy} = \frac{E}{1-\nu^2}\left(\frac{\partial v}{\partial y} + \nu \frac{\partial u}{\partial x}\right)$$

and $u(x,y)$ are displacements in the x- and y-directions and E is the elastic modulus, ν is the Poisson's ratio. In the calculations, we set $E = 1000$, $\nu = 0.3$ as in [Zhang, Song, Lu, and Liu (2000)]. As boundary conditions, the displacements defined by the exact solutions were used. They were approximated at nodal points which were distributed in the same manner as those in the above cited publications.

Different strategies of forming stencils were tried. One way was as follows. For each center $\mathbf{x}_j$, the stencil was defined as a set of nodes which fall on a domain $S_j : \mathbf{x}_j \in S_j$ with a prescribed shape of its boundary and a prescribed characteristic length R (the latter was, for example, a circle radius, the edge of a rectangular etc.) or a characteristic area. Uniform nodal distributions were used, M and N nodes being placed in the radial and azimuthal directions.

Two types of stencils were assigned to the nodes in the below presented example, the supports being shown in Fig. 6. They were squares with the characteristic length R as well as the "patches" defined in the polar coordinates (r,ϕ) by $r_0 - R < r < r_0 + R, \quad \phi_0 - \Delta\phi < \phi < \phi_0 + \Delta\phi$ where $\Delta\phi = 20^\circ$.

Fig. 6 shows the relative m.r.s. displacements error E_{uv} for three uniform nodal distributions ($4 \times 7,\ 7 \times 10,\ 13 \times 19$) as functions of R. As seen in the Figure, the solution errors decrease with increasing R for a fixed $M \times N$ mesh if $R < R_*(M,N)$ where $R_*(M,N)$ is a "saturation" value. Further increase of R for fixed M and N does not reduce the errors since enlarging stencils is not accompanied by increasing density of the nodes. The behaviour

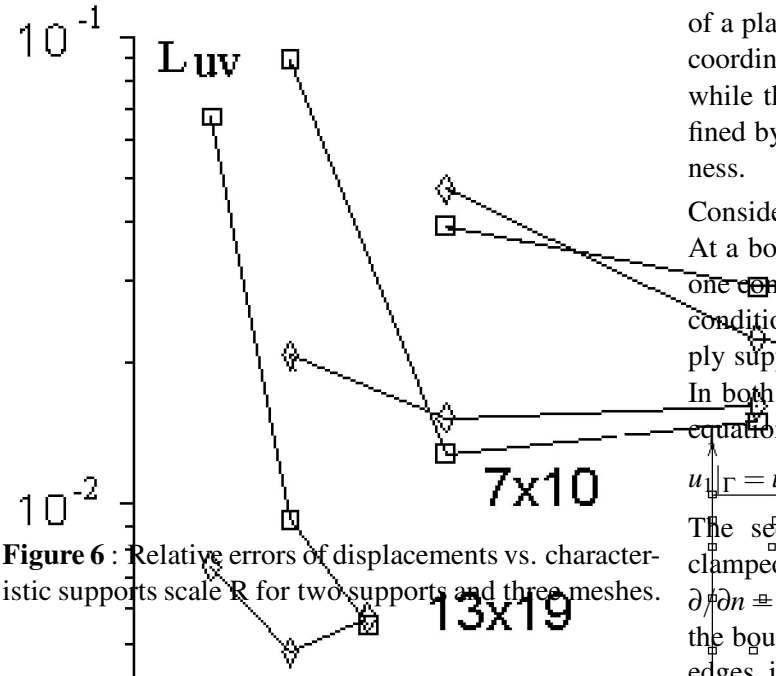

Figure 6 : Relative errors of displacements vs. characteristic supports scale R for two supports and three meshes.

of the "minimal" errors $E_m = E_{uv}(R_*)$ when refining the meshes (that is, when increasing the density of nodes) is also shown in Fig. 6.

Non-linear shell equations. The present RBF technique can be readily applied to more complicated PDE's. As an example, we consider a non-linear shell problem described by the Karman-Fopple equations. They read [Grigoluk and Mamai (1997)].

$$\frac{\partial^2 u_1}{\partial x^2}+\frac{\partial w}{\partial x}\frac{\partial^2 w}{\partial x^2}+\frac{1+\nu}{2}\left(\frac{\partial^2 u_2}{\partial x\partial y}+\frac{\partial w}{\partial y}\frac{\partial^2 w}{\partial x\partial y}\right)+$$

$$+\frac{1-\nu}{2}\left(\frac{\partial^2 u_1}{\partial y^2}+\frac{\partial w}{\partial x}\frac{\partial^2 w}{\partial y^2}\right)=0$$

$$\frac{\partial^2 u_2}{\partial y^2}+\frac{\partial w}{\partial y}\frac{\partial^2 w}{\partial y^2}+\frac{1+\nu}{2}\left(\frac{\partial^2 u_1}{\partial x\partial y}+\frac{\partial w}{\partial x}\frac{\partial^2 w}{\partial x\partial y}\right)+$$

$$+\frac{1-\nu}{2}\left(\frac{\partial^2 u_2}{\partial x^2}+\frac{\partial w}{\partial y}\frac{\partial^2 w}{\partial x^2}\right)=0$$

$$D\triangle\triangle w=q+\frac{Eh}{1-\nu^2}\left[\left(\frac{\partial u_1}{\partial x}+\nu\frac{\partial u_2}{\partial y}+\frac{1}{2}\left(\frac{\partial w}{\partial x}\right)^2+\right.\right.$$

$$+\frac{\nu}{2}\left(\frac{\partial w}{\partial y}\right)^2\Bigg)\frac{\partial^2 w}{\partial x^2}+\left(\frac{\partial u_2}{\partial y}+\nu\frac{\partial u_1}{\partial x}+\frac{1}{2}\left(\frac{\partial w}{\partial y}\right)^2+\right.$$

$$\left.\left.\frac{\nu}{2}\left(\frac{\partial w}{\partial x}\right)^2\right)\cdot\frac{\partial^2 w}{\partial y^2}+(1-\nu)\left(\frac{\partial u_1}{\partial y}+\frac{\partial u_2}{\partial x}+\frac{\partial w}{\partial x}\frac{\partial w}{\partial y}\right)\frac{\partial^2 w}{\partial x\partial y}\right]$$

In the above equations, u_1, u_2, w are the displacements of a plate middle surface corresponding to the Cartesian coordinates x, y, z respectively. q is a loading function while the coefficient D, the cylindrical stiffness, is defined by $D = Eh^3/(12(1-\nu^2))$, h being the shell thickness.

Consider now the boundary conditions for the system. At a boundary point, four conditions are needed, that is one condition for each of the first two equations and two conditions for the third equation. In the following, simply supported edges or clamped edges will be assumed. In both cases, the boundary conditions for the first two equations and the condition for the third equation look as

$$u_1|_\Gamma = u_2|_\Gamma = w|_\Gamma = 0$$

The second condition for the third equation in the clamped edges case has the form $\partial w/\partial n = 0$ where $\partial/\partial n = 0$ is the operator of the derivative in the normal to the boundary direction. In the case of simply supported edges, it reads

$$\triangle w+(1-\nu)k\partial w/\partial n = 0$$

where k is the curvature of the boundary.

In the calculations, an unstructured triangulated grid was used.

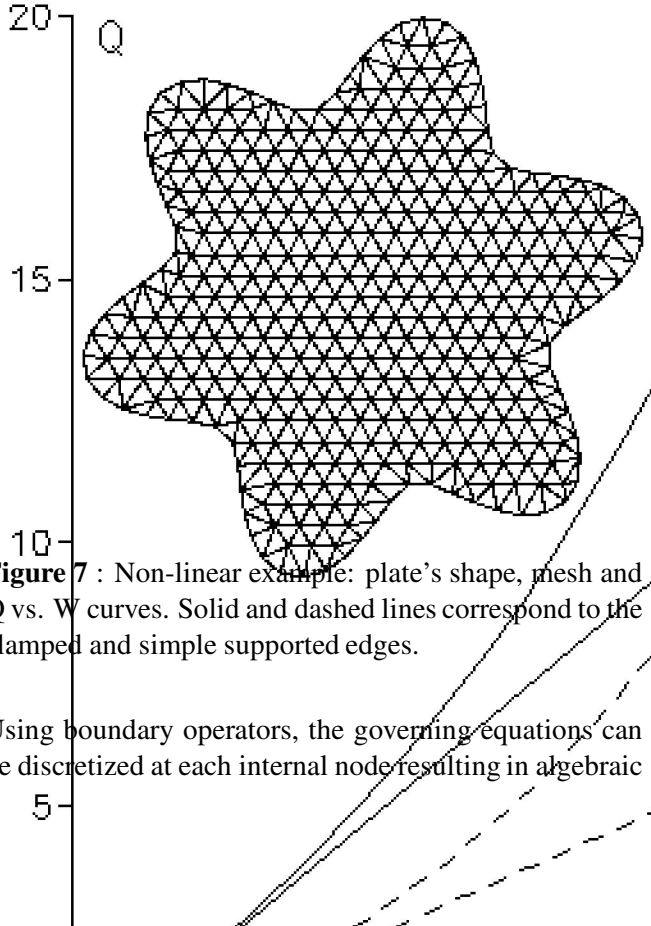

Figure 7 : Non-linear example: plate's shape, mesh and Q vs. W curves. Solid and dashed lines correspond to the clamped and simple supported edges.

Using boundary operators, the governing equations can be discretized at each internal node resulting in algebraic

systems for the vector-valued nodal functions u_1, u_2 and W which can be cast in the form

$$L_{11}u_1^{n+1} + L_{12}u_2^{n+1} = f_1(w^n)$$

$$L_{21}u_1^{n+1} + L_{22}u_2^{n+1} = f_2(w^n)$$

$$Lw^{n+1} = f(u_1^{n+1},\ u_2^{n+1},\ w^n)$$

where L_{11}, L_{12}, L_{21}, L_{22}, L are the operators approximating linear parts of the equations while the right hand sides contain non-linear operators, n being the iteration count. Thus, the solution procedure consists of solving the linear systems for u_1 and u_2 during $(n+1)$th iteration with known w^n values, calculating f in the third equation and, finally, solving the linear system for w^{n+1}.

As an example of calculations for more complicated geometry than that in the previous testing problem, Fig. 7 presents the dependence W vs. Q where W and Q are dimensionless vertical displacement and loading function respectively. The plate boundary is given by $r = R(1+\cos(6\phi)/5)$ in the polar coordinates (r,ϕ), the nodes distribution being shown in the Figure. One can see considerable difference of the results obtained in the frameworks of linear and non-linear theory.

4.3. Solving advection and Navier-Stokes equations

In general, advection and advection-diffusion type of equations are more difficult cases when using RBF schemes due to presence of skew-symmetric differential operators. To meet stability requirements, some care should be exercised when choosing neighbor nodes around center nodes. The stencils investigated in Subsection 3.2 are appropriate from the stability viewpoint. However, their first order accuracy impels one to look for enlarged stencils allowing stable calculations. We present an example of using approach described in the Subsection 3.4. It consists of calculating the relevant RBF coefficients for p nodal points by solving linear systems with $l \times p$ $(l < p)$ matrices and obtaining values $p-l$ free parameters by applying the least square principle.

Advection equation with varying coefficients. As a test problem consider the equation

$$\frac{\partial u}{\partial t} + y\frac{\partial u}{\partial x} - x\frac{\partial u}{\partial y} = 0$$

in the domain $1 < r < 2$, $r = \sqrt{x^2+y^2}$, with the boundary conditions $\partial u/\partial r|_{r=1} = \partial u/\partial r|_{r=2} = 0$ and the initial data

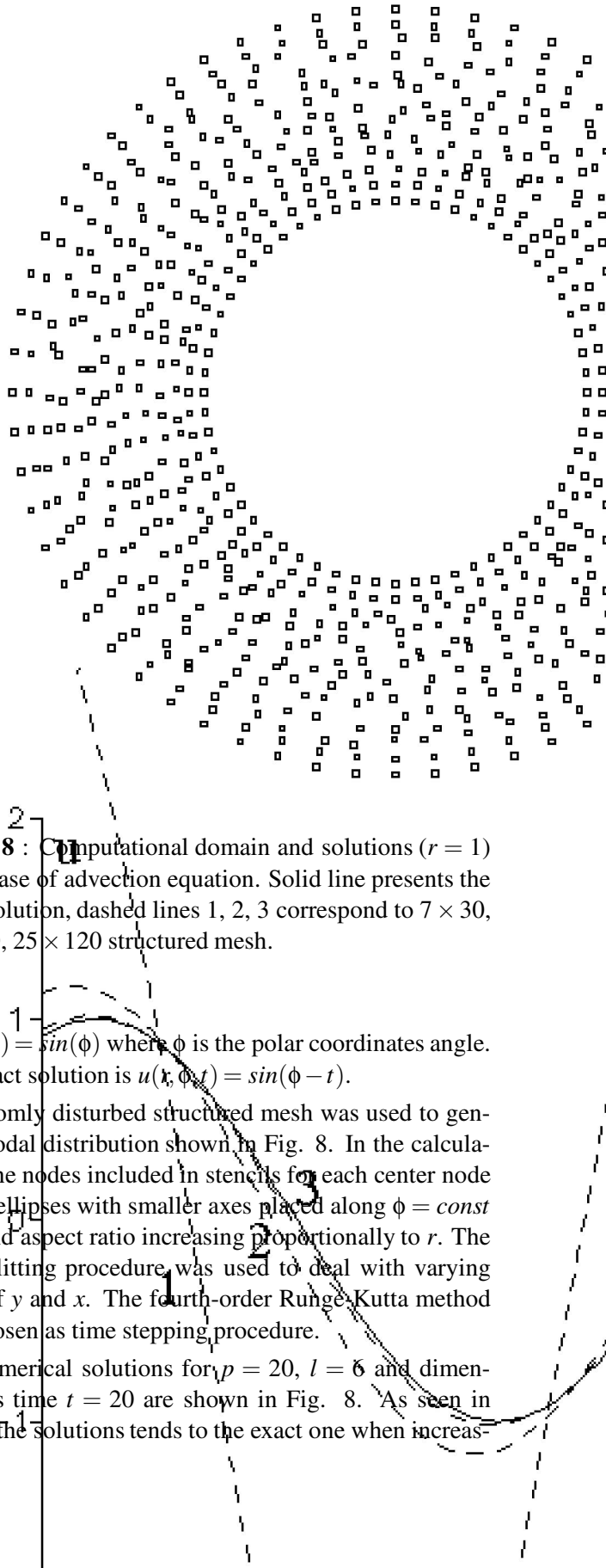

Figure 8 : Computational domain and solutions $(r = 1)$ in the case of advection equation. Solid line presents the exact solution, dashed lines 1, 2, 3 correspond to 7×30, 13×60, 25×120 structured mesh.

$u(r,\phi,0) = sin(\phi)$ where ϕ is the polar coordinates angle. The exact solution is $u(r,\phi,t) = sin(\phi - t)$.

A randomly disturbed structured mesh was used to generate nodal distribution shown in Fig. 8. In the calculations, the nodes included in stencils for each center node fall on ellipses with smaller axes placed along $\phi = const$ lines and aspect ratio increasing proportionally to r. The flux splitting procedure was used to deal with varying signs of y and x. The fourth-order Runge-Kutta method was chosen as time stepping procedure.

The numerical solutions for $p = 20$, $l = 6$ and dimensionless time $t = 20$ are shown in Fig. 8. As seen in Fig. 8, the solutions tends to the exact one when increas-

ing the density of nodes. The convergence order can be estimated to be about two.

The Navier-Stokes calculations Applications of meshless methods to incompressible Navier-Stokes equations are reported in [Lin and Atluri (2001)], [Shu,Ding and Yeo(2003)]. We consider here compressible gas flows described by Navier-Stokes equations and characterized by large Reynolds numbers. In this case, the skew-symmetric differential operators in non-lnear terms are dominating outside boundary layers and RBF stencils should be constructed to provide stable time-stepping or iteration processes. Several types of stencils were suggested, and, in particular, those which use nodes from elliptical supports with a proper space orientation. Preliminary results of the Navier-Stokes calculations are shown in Fig. 9 and 10.

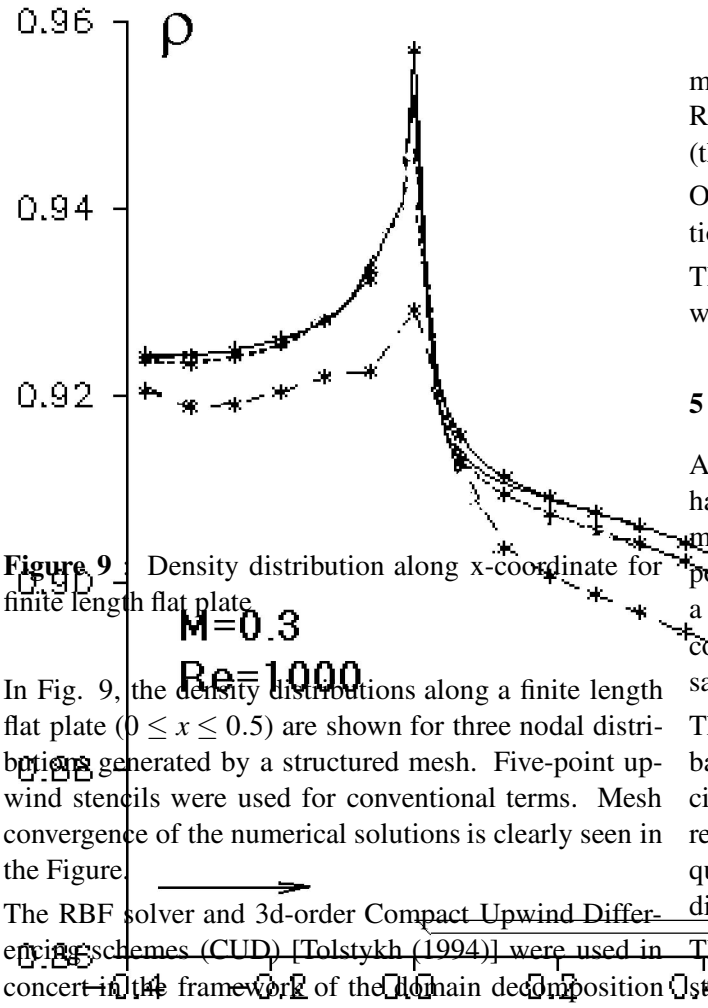

Figure 9 : Density distribution along x-coordinate for finite length flat plate

In Fig. 9, the density distributions along a finite length flat plate ($0 \leq x \leq 0.5$) are shown for three nodal distributions generated by a structured mesh. Five-point upwind stencils were used for conventional terms. Mesh convergence of the numerical solutions is clearly seen in the Figure.

The RBF solver and 3d-order Compact Upwind Differencing schemes (CUD) [Tolstykh (1994)] were used in concert in the framework of the domain decomposition strategy, the RBF domain near the leading edge being shown in Fig. 10. The density distribution along the normal direction at the stagnation point are obtained using RBF stencils "1)" and "2)" and the CUD scheme alone (the line with markers).

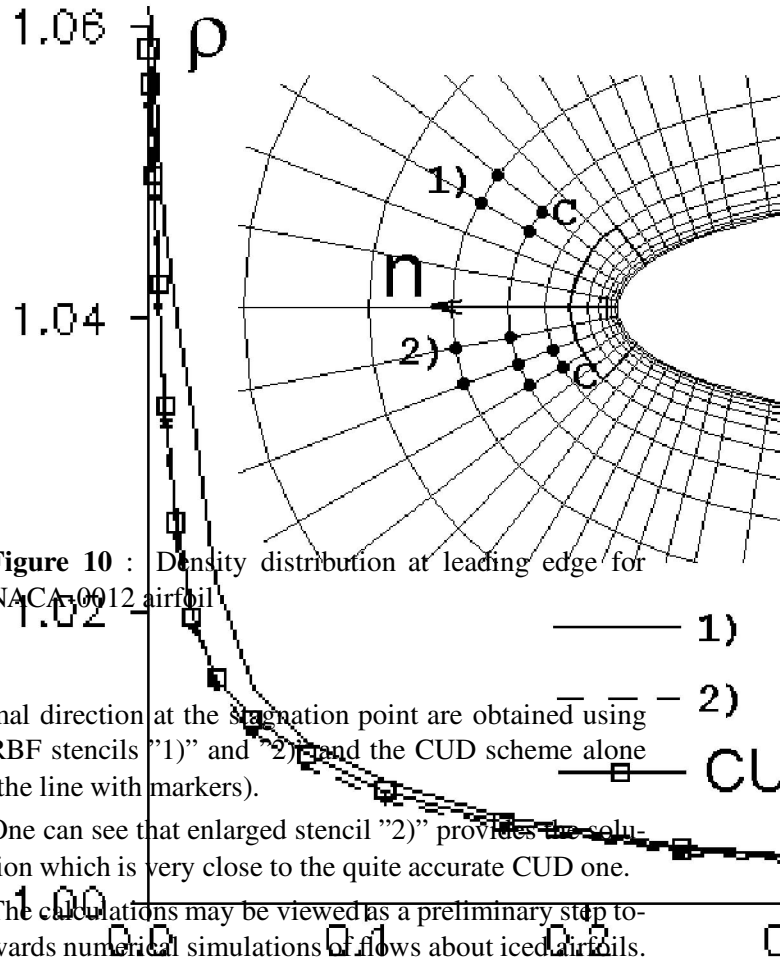

Figure 10 : Density distribution at leading edge for NACA-0012 airfoil

One can see that enlarged stencil "2)" provides the solution which is very close to the quite accurate CUD one.

The calculations may be viewed as a preliminary step towards numerical simulations of flows about iced airfoils.

5 Conclusions

A way of using radial basis functions for solving PDEs has been described. Its essence is constructing approximations to derivatives at each node based on RBF interpolants for a limited number of neighbour nodes forming a stencil in the finite-difference sense. In contrast to the collocation approach, PDEs are approximated rather than satisfied at nodes in computational domains.

The approach has the potential for minimizing the drawback related to ill-conditioned systems for RBF coefficients and providing reasonable solutions accuracy for relatively modest numbers of nodes. It allows one to be quite flexible by choosing stencils for distinct nodes and different types of derivatives.

The finite difference concepts concerning approximation, stability and convergence are formulated for the present RBF schemes. In the case of the simplest RBF discretizations of the Poisson and advection equations, approxima-

tions and stability proofs are presented

The technique has been applied to several elasticity problems. The numerical experiments confirmed the above theoretical expectations. Comparisons with the exact solutions showed that quite accurate numerical solutions can be obtained using relatively low-density nodal distributions.

Examples of the RBF solutions of the compressible Navier-Stokes equations are also presented showing the applicability of the technique to non-linear problems with non-selfadjoint operators.

Further investigations into operating properties of the RBF "finite difference mode" are needed. In particular, optimal strategies of defining stencils can be viewed as the subject of the study.

Acknowledgment: This work was supported by Russian Fund of Basic researches (grant 02-01-00436) and INTAS (project 1150)

References

Atluri S.N (2004): *The Meshless Method (MLPG) for Domain and BIE Discretizations*, Tech Science Press.

Atluri S. N.; Han Z.D.; A. M. Rajendran A.M. (2004): A New Implementation of the Meshless Finite Volume Method, Through the MLPG "Mixed" Approach. *CMES: Computer Modeling in Engineering & Sciences*, vol. 6, No. 6, pp. 491-514.

Atluri S.N.; Shen S. (2002): The Meshless Local Petrov-Galerkin (MLPG) Method: A Simple Less-costly Alternative to the Finite Element and Boundary Element Methods. *CMES: Computer Modeling in Engineering & Sciences*, vol. 3, No. 1, pp. 11-52.

Atluri, S.N.; Zhu,T.-L.(2000): The meshless local Petrov-Galerkin (MLPG) approach for solving problems in elasto-statics, *Comput. Mech.*, vol. 25, pp. 169-179.

Babuska, I.; Scapolla, T. (1989): Benchmark computation and performance evaluation for a rhombic plate bending problem. *Int. J. Num. Meth. Eng.*, vol. 28, pp. 155-179.

Belotserkovskii O.M.; Kholodov A.S. (1999): Majorizing schemes on unstructured grids in the space indeterminate coefficients. *Comput. Math. and Math. Phys.*, vol. 39, pp. 1730-1747.

Belytchko T.; Krongaus Y.; Organ D.; Fleming M.; Krysl P. (1996): Meshless methods: An overview and recent developments. *Comp. Meth. Appl. Eng.*, vol. 139, pp. 3-47.

Buhmann, M.D. (1998): Radial functions on compact support. *Proc. Edinburg Math. Soc.*, vol. 41, pp. 33-46.

D'yachenko V.F. (1965): A new method for the numerical solution of non-stationary problems of gas dynamics with two spatial variables. *Zh Vycisl. Mat. mat. Fiz.*, vol. 5, pp. 680-688.

Fasshauer, G. (1996): Solving partial differential equations with collocation with radial basis functions. In: LeMehaute A., Robut C. and Shumaker L.L. (eds.), *Chamonix proceedings*, Vanderbilt University Press, Nashville TN, pp.1-8.

Franke, C.; Schaback, R. (1998): Solving partial differential equations by collocation using radial basis functions. *Appl. Math. Comput.*, vol. 93, pp. 73-82.

George, A.; Liu, J.W-H (1981): *Computer Solution of Large Sparse Positive Definite Systems*, New Jercey, Prentice-Hall.

Godunov, S.K.; Ryaben'kii, V.S. (1977): *Difference scheme*, Moscow, Nauka.

Grigoluk, E.I.; Mamai, V.I. (1997): *Unlinear deformation of thin-wall constructions*, Moscow: Nauka Fizmatlit.

Han Z. D.; and Atluri S. N. (2004): Meshless Local Petrov-Galerkin (MLPG) approaches for solving 3D Problems in elasto-statics. *CMES: Computer Modeling in Engineering & Sciences*, vol. 6, No. 2, pp. 169-188.

Hardy, R.L. (1990): Theory and applications of multiquadric-biharmonic method. *Comput. Math. Appl.*, vol. 19, pp. 163-208.

Kansa, E.J. (1990): Multiquadrics - a scattered data approximation scheme with applications to fluid dynamics - II: Solutions to parabolic, hyperbolic and elliptic partial differential equations *Comput. Math. Appl.*, vol. 19, pp. 147-161.

Kansa E.J., Carlson R.E. (1995): Radial basis function: a class of grid-free scattered data approximations. *Comput. fluid dynamics J.* vol. 3, pp. 479-496.

Kansa, E.J.; Hon, Y.C. (2000): Circumventing the ill-conditioning problem with multiquadric radial basis functions: Applications to elliptic partial differential equations. *Comp. Math. Appl.*, vol. 39, pp. 123-137.

Lin, H.; Atluri S.N. (2001): The Meshless Local Petrov-Galerkin (MLPG) Method for Solving Incompressible

Navier-Stokes Equations, *CMES: Computer Modeling in Engineering & Sciences* vol. 2, No. 2, pp. 117-142.

Lizka T., Orkitz J. (1980): The finite difference method at arbitrary irregular grids and its application in applied mechanics. *Comput. Struct.* vol. 11, pp. 83-95.

Madych W.R., Nelson S.A. (1989): Error bounds for multiquadric interpolation. *In Approximation theory VI*, Chui C.K., Shumaker L.L., Wards J.W.(eds), Academic Press, NY

Micchelli C.A. (1986): Interpolation of scattered datra distance matrices and conditionally positive definite functions *Constr.Approx*, vol. 2, pp. 11-22.

Sharan, M.; Kansa, E.J.; Gupta, S. (1997): Applications of the multiquadric method for the solution of elliptic partial differential equations. *Appl. Math. Comput.* vol. 84, pp. 275-302.

Shu, C.; Ding, H.; Yeo K.S. (2003): Local radial basis functions-based differential quadrature method and its application to solve two-dimensional incompressible Navier-Stokes equations, *Comput. Methods Appl. Mech. Engng.*, vol. 192, pp. 941-954.

Tolstykh, A.I. (1994): *High accuracy non-centered compact difference schemes for fluid dynamics applications*, World Scientific, Singapore.

Tolstykh, A.I. (2000): On using RBF-based differencing formulas for unstructured and mixed structured-unstructured grid calculations. In *Proceedings of 16th IMACS World Congress (CD)*, Lausanne.

Tolstykh, A.I. (2003): On multioperators principle for constructing arbitrary-order difference scheme. *Appl. Num. Math.*, vol. 46, pp. 411-423.

Tolstykh, A.I.; Shirobokov, D.A. (2003): On using radial basis functions in a "finite difference mode" with applications to elasticity problems. *Comput. Mech.*, vol. 33, pp. 68-79.

Vlasov, V.I.; Volkov, D.B. (1995): Multypole method for solving Poisson equation in domains with rounded angles. *Zh. Vychisl. Mat. Mat. Fiz.* vol. 35, pp. 867-872.

Wendland, H. (1995): Piecewise polynomial, positive definite and compactly supported radial basis functions of minimal degree. *Adv. Comput. Math.*, vol. 4, pp. 386-396.

Wong, S.M.; Hon, Y.C.; Li, T.S.; Chung, S.L.; Kansa, E.J. (1999): Multizone decomposition of time dependent problems using the multiquadric scheme. *Comput. Math. Appl.*, vol. 37(8), pp. 23-43.

Wu, Z. (1995): Compactly supported positive definite radial functions. *Adv. Comput. Math.*, vol. 4, pp. 283-292.

Wu, Z.; Shaback, R. (1993): Local error estimates for radial basis function interpolation of scattered data. *IMA J. Numer. Anal.*, vol. 13, pp. 13-27.

Wu, Z. (1998): Solving PDE with radial basis function and the error estimation. In: Chen Z., Li Y., Micchelli C.A., Xu Y., Dekker M., Guang Zhou (eds.) *Advances in Computational Mathematic Lecture Notes on Pure and Applied Mathematics*, pp. 202.

Zerroukat, M.A. (1998): Fast boundary element algorithm for time-dependant potential problems. *Appl. Math. Modelling.* vol. 22, pp. 183-196.

Zhang, X.; Song, K.Z.; Lu, M.W.; Liu, X. (2000): Meshless methods based on collocation with radial basis functions. *Comput. Mech.* vol. 26, pp. 333-343.